Review

Significance of Histidine Hydrogen–Deuterium Exchange Mass Spectrometry in Protein Structural Biology

Masaru Miyagi [1],* and Takashi Nakazawa [2],*

1   Department of Pharmacology, Case Western Reserve University, 10900 Euclid Avenue, Cleveland, OH 44106-4988, USA
2   Department of Chemistry, Nara Women's University, Nara 630-8506, Japan
*   Correspondence: masaru.miyagi@case.edu (M.M.); t.nakazawa@cc.nara-wu.ac.jp (T.N.)

Simple Summary: Various techniques are at our disposal for probing the structure and dynamics of proteins. Mass spectrometry stands out prominently in this realm due to its exceptional detection specificity and sensitivity. This enables the precise identification of individual molecular species in complex mixtures with remarkable sensitivity. The unique strengths of mass spectrometry have spurred the development of numerous approaches for characterizing protein molecules. In this review, our focus is on a specific mass-spectrometry-based method known as histidine hydrogen–deuterium exchange mass spectrometry (His-HDX-MS). We delve into its principle, experimental workflow, applications and the details of data analysis and interpretation.

Abstract: Histidine residues play crucial roles in shaping the function and structure of proteins due to their unique ability to act as both acids and bases. In other words, they can serve as proton donors and acceptors at physiological pH. This exceptional property is attributed to the side-chain imidazole ring of histidine residues. Consequently, determining the acid-base dissociation constant (K_a) of histidine imidazole rings in proteins often yields valuable insights into protein functions. Significant efforts have been dedicated to measuring the pK_a values of histidine residues in various proteins, with nuclear magnetic resonance (NMR) spectroscopy being the most commonly used technique. However, NMR-based methods encounter challenges in assigning signals to individual imidazole rings and require a substantial amount of proteins. To address these issues associated with NMR-based approaches, a mass-spectrometry-based method known as histidine hydrogen–deuterium exchange mass spectrometry (His-HDX-MS) has been developed. This technique not only determines the pK_a values of histidine imidazole groups but also quantifies their solvent accessibility. His-HDX-MS has proven effective across diverse proteins, showcasing its utility. This review aims to clarify the fundamental principles of His-HDX-MS, detail the experimental workflow, explain data analysis procedures and provide guidance for interpreting the obtained results.

Keywords: histidine; histidine protonation; acid dissociation constant; mass spectrometry; protein structural biology

1. Introduction

Histidine (His) residues exhibit exceptionally diverse features in protein functions, including catalysis, hydrogen bonding and metal binding. The distinctive chemical properties of His residues stem from their side-chain imidazole group, which bears two nitrogen atoms at N-1 (δ2) and N-3 (δ1) positions (Figure 1) [1]. These nitrogen atoms play crucial roles in the functions of His residues, serving either as hydrogen acceptors or donors in the two tautomeric forms of the imidazole group (Im), depending on the position of the hydrogen atom attached to either the N-1 or N-3 position. Importantly, either form of the imidazole group can act as a base and acquire a proton to become the cationic imidazolium

group (Im·H$^+$), which is stabilized by the resonance structure between its two tautomeric forms (Scheme 1).
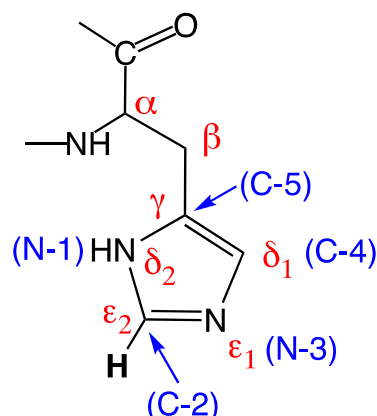
Figure 1. Atom nomenclature of histidine residue. Greek letters (in red) are typically employed to denote the atomic positions of a histidine residue. Alternatively, a numbering system is often used to specify the atomic positions of the histidine imidazole ring, as shown in blue.
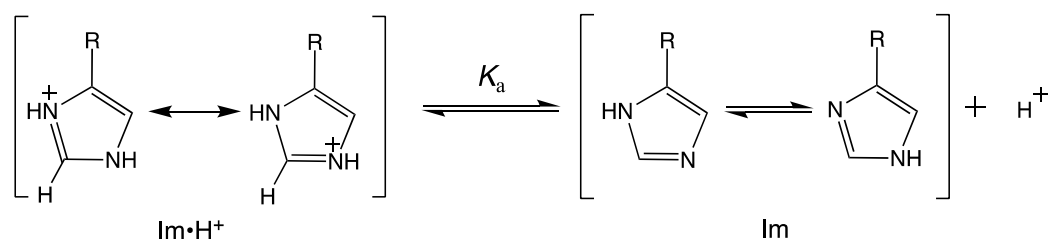
Scheme 1. Acid-base equilibrium between the imidazole group (Im) and the imidazolium group (Im·H$^+$) with the dissociation constant K_a. The equilibrium arrows ($\rightleftharpoons$) signify that the two species on each side are in equilibrium, while the resonance arrow ($\leftrightarrow$) suggests that the two species on either side are resonance structures of each other.

The dissociation constant of this acid-base equilibrium, K_a, is expressed in the following equation:

$$K_a = \frac{[\text{Im}]\left[\text{H}^+\right]}{\left[\text{Im·H}^+\right]} \quad (1)$$

where [Im], $\left[\text{H}^+\right]$ and $\left[\text{Im·H}^+\right]$ denote the concentrations of imidazole, proton and imidazolium, respectively. For simplification, we often use the pK_a value, which directly correlates with the pH of an aqueous solution. This connection is established by taking the logarithm of both sides of Equation (1), as shown below:

$$\text{p}K_a = -\log_{10}\frac{[\text{Im}]}{\left[\text{Im·H}^+\right]} + \text{pH} \quad (2)$$

The pK_a value of the imidazole group in proteins can vary widely (from approximately 4 to 9) depending on its electrostatic environment [2–4]. This distinctive property enables His residue to engage in diverse catalytic processes, functioning either as an acid or a base. Even within a single catalytic process, the imidazole groups are capable of functioning as both proton donors (acid) and acceptors (base) in different catalytic steps, as seen in the catalysis of serine proteases [5–7]. Furthermore, this unique property facilitates the binding of His residues with metals over a considerably wide pH range. Consequently, the precise measurement of pK_a values in His residues is often crucial to understanding the mechanism of enzyme reactions.

Until recently, nuclear magnetic resonance (NMR) spectroscopy has been by far the most widely used technique for determining the pK_a values of His residues in proteins [5,8,9]. However, NMR-based approaches have significant drawbacks, including difficulties in assigning signals to individual His residues in proteins and the requirement for a large quantity of proteins. To address the challenge of signal assignment and detection sensitivity, a mass-spectrometry (MS)-based method called histidine hydrogen–deuterium exchange mass spectrometry (His-HDX-MS) was developed in 2008 [10]. Since then, His-HDX-MS has been demonstrated to overcome the limitations of NMR-based approaches and has proven to be useful not only in determining the pK_a values of His residues but also in probing the conformational changes in proteins.

In this review, we begin by elucidating the foundational principles of His-HDX-MS. Subsequently, we detail the experimental workflow, explore the applications of this method, outline data analysis procedures and provide guidance on interpreting the results.

2. pK_a Value and Kinetic Parameters of the Acid-Base Equilibrium of His Residues in Proteins

2.1. Measurement of pK_a with NMR Spectroscopy

Until recently, NMR spectroscopy has been by far the most widely used technique for determining the pK_a values of His residues in proteins [5,8,9,11,12]. The most advantageous feature of NMR is that the ^{1}H and ^{13}C signals of the imidazole C-2 position (Figure 1) are well resolved from the majority of other resonances, even in one-dimensional spectra. The chemical shift in C-2 signal observed at δ_{obs} (ppm) reflects the weighted average of limiting chemical shits δ_{Im} and $\delta_{Im \cdot H+}$ of the imidazole group in non-protonated (Im) and protonated (Im·H$^+$) forms, respectively (Figure 2). The differences in chemical shifts $\delta_{Im \cdot H+} - \delta_{obs}$ and $\delta_{obs} - \delta_{Im}$ are proportional to concentrations [Im] and $\left[\text{Im·H}^+ \right]$, respectively. Therefore, pK_a can be expressed in an equation replacing the $\left[\text{Im·H}^+ \right]/[\text{Im}]$ term of the Henderson–Hasselbalch equation (Equation (2)) with $(\delta_{ImH+} - \delta_{obs})/(\delta_{obs} - \delta_{Im})$, as follows:

$$\mathrm{p}K_a = -\log_{10}\frac{(\delta_{\mathrm{Im \cdot H+}} - \delta_{\mathrm{obs}})}{(\delta_{\mathrm{obs}} - \delta_{\mathrm{Im}})} + \mathrm{pH} \qquad (3)$$
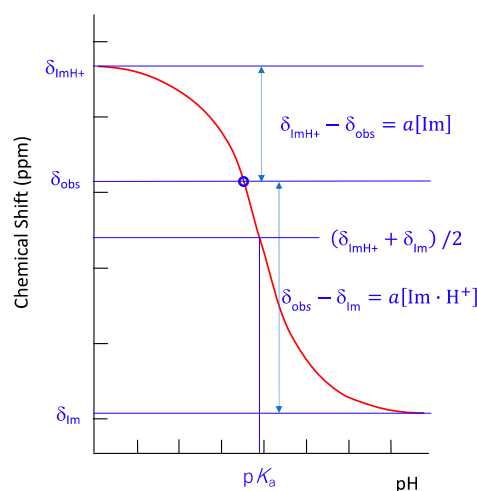

Figure 2. The idealized NMR titration curve (red line) of His C-2 proton resonance. The variations in chemical shifts, denoted by the distances between blue lines ($\delta_{Im \cdot H+}$ and δ_{obs}, and δ_{obs} and δ_{Im}), scale proportionally with the concentrations $[Im]$ and $\left[Im \cdot H^+ \right]$, respectively. The midpoint of the titration curve is represented by $(\delta_{Im \cdot H+} + \delta_{Im})/2$.

Although this method is simple and easy to perform, difficulties persist in unambiguously assigning ^{1}H, ^{13}C and ^{15}N signals to individual C-2 resonances, even in a small protein containing only a few His residues. In principle, it is still possible to assign every C-2 signal to the relevant His residue using sophisticated multi-dimensional NMR techniques.

For example, the pK_a values of seven His residues in human carbonic anhydrase II (29 kDa) have been determined via pH titration of selectively enriched ^{15}N signals of imidazole N-1 and N-3 atoms, which were assigned by a combination of multi-dimensional heteronuclear correlation spectroscopy [13]. However, the necessity to prepare ^{13}C- and ^{15}N-labeled recombinant proteins at a considerably high concentration (1–3 mM) represents a significant limitation of the method's applicability to larger proteins [8,13]. Furthermore, preparing isotope-labeled large proteins in large quantities is expensive and time consuming.

2.2. Measurement of pK$_a$ and Kinetic Parameters Using Tritium Labeling

Prior to the invention of electrospray ionization (ESI) mass spectrometry, tremendous efforts were made by Matsuo and colleagues to address the drawbacks of NMR-based approaches using tritium (^{3}H or T) labeling [14,15]. In this method, proteins were incubated in buffers at various pH values containing tritiated water (^{3}H$_2$O) for ~2 days. Subsequently, the proteins were digested using a combination of proteases, and the resulting peptides were separated through two-dimensional paper chromatography electrophoresis. The radioactive spots were then excised, and their radioactivities were measured. The identity of the radioactive peptides was determined through amino acid analysis. Although this tritium labeling method based on hydrogen–tritium exchange (HTX) reaction successfully alleviated the problems of NMR experiments by achieving much higher sensitivity and the accurate assignment of tritium-incorporated His residues, its technical complexity was daunting to the majority of researchers, except for a few peptide chemists. In fact, a seminal textbook on protein science referred to this method as follows: "These experiments are tedious to perform, but the assignments of pK_a are unambiguous" [16].

2.3. Measurement of pK$_a$ and Kinetic Parameters Using MS

To address the challenges associated with NMR signal assignment, Miyagi and Nakazawa proposed employing ESI mass spectrometry [10]. Their successful demonstration revealed that this mass-spectrometry-based approach effectively resolves signal assignment issues encountered in NMR spectroscopy and significantly reduces the quantity of protein required. In the following sections, we delve into the mechanism of HDX reaction at the imidazole ring of His residues (Section 2.3.1), the calculation methods for obtaining the HDX rate constant from the acquired mass spectrum (Section 2.3.2) and the relationship between pK_a values and HDX rates (Section 2.3.3).

2.3.1. The Mechanism of HDX Reaction at the C-2 Position of the Imidazole Group

Hydrogens, which are covalently attached to nitrogen, oxygen or sulfur atoms, exchange rapidly with deuterium atoms in D$_2$O solvent. Additionally, the C-2 hydrogen of the imidazole ring of His residues exchanges with deuterium but at a much slower rate, with a half-life in the order of days at ambient temperature [17,18]. The C-2 hydrogen is the only hydrogen in proteins, which is covalently bonded to a carbon atom but still exchanges with the hydrogen of aqueous solvents.

The HDX reaction at the C-2 position of the His imidazole ring has been established as a base-catalyzed process involving the abstraction of a proton from the C-2 position of the imidazolium ion [Im·D$^+$] to form an ylide in the rate-determining step [19–22] (Scheme 2). Therefore, the rate of reaction can be expressed in the following equation using the second-order rate constant, k_2, and concentrations of the imidazolium ion [Im·D$^+$] and deuteroxide ion $\left[\text{OD}^-\right]$.

$$\text{rate} = k_2 \left[\text{Im·D}^+\right]\left[\text{OD}^-\right] \tag{4}$$

Given that the overall reaction adheres to pseudo-first-order kinetics [20], and the rate is solely dependent on the concentration of the imidazole group, [Im$_{\text{total}}$], the rate equation can also be expressed as

$$\text{rate} = k_\varphi \left[\text{Im}_{\text{total}}\right] \tag{5}$$

where k_φ is the pseudo-first-order rate constant. Rearrangement of Equations (4) and (5) yields the following expression:

$$k_\varphi = \frac{k_2 K_W}{(K_a + [D^+])} \tag{6}$$

Here, K_a represents the dissociation constant of imidazolium cation ($K_a = [\text{Im}][D^+]/[\text{Im}\cdot D^+]$), and K_W represents the ion product of water ($K_W = [D^+][OD^-]$), with a value of $10^{-14.87}$ [23]. As the pH increases, the value of k_φ approaches its maximum value, $k_\varphi^{\max}$. Under conditions where $K_a >> [D^+]$, $k_\varphi^{\max}$ is expressed by the equation

$$k_\varphi^{\max} = \frac{k_2 K_W}{K_a} \tag{7}$$

Using Equation (7) with experimentally obtained pK_a and $k_\varphi^{\max}$ values, one can estimate the second-order rate constant k_2. Plugging the estimated value of k_2 with varying concentrations of $[D^+]$ into Equation (6) allows one to simulate the theoretical HDX titration curve of a given imidazole ring. Figure 3 shows the ribonuclease A (RNase A) His12 titration curve obtained previously (blue line) [10] and its theoretical curve calculated using Equation (6) (red line), demonstrating that the experimental data and theoretical data based on the reaction mechanism agree well.
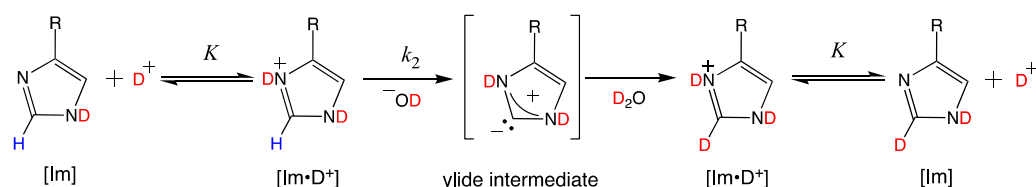
Scheme 2. The mechanism of HDX reaction at the C-2 position of the imidazole group. The rate-determining step corresponds to the base-catalyzed abstraction of the C-2 proton of the imidazolium group (Im·D$^+$) to form an ylide intermediate. In this scheme, the possible resonance hybrid of the ylide—a carbene—is omitted for simplicity. Protons (H) and deuterons (D) are shown in blue and red letters, respectively.
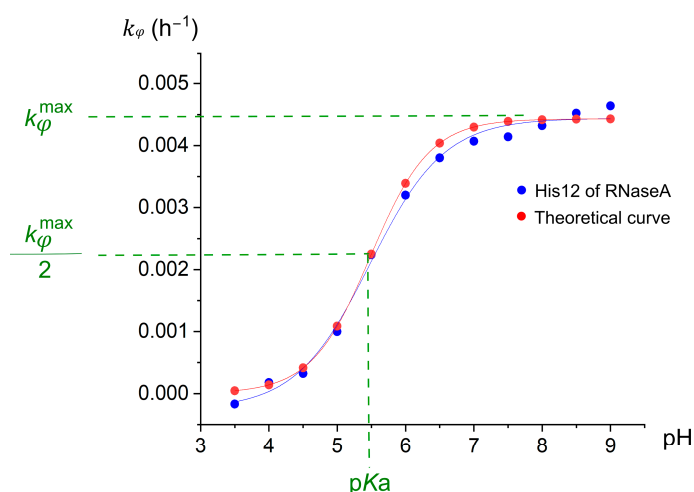

Figure 3. The pH titration curve of His12 of RNase A and its theoretical curve calculated using Equation (6).

2.3.2. Calculation of the Pseudo-First-Order Rate Constant k_φ from a Mass Spectrum

The pseudo-first-order rate constant k_φ can be obtained directly from the acquired mass spectrum. Figure 4 shows the hypothetical mass spectra of a peptide containing

one histidine residue before (red) and after (blue) HDX reaction. The intensities of M and M + 1 peaks before HDX reaction, $I_M(0)$ and $I_{M+1}(0)$, respectively, could change to $I_M(t)$ and $I_{M+1}(t)$ after the reaction incorporating deuterium. Since the HDX reaction follows first-order kinetics, the changes in I_M and I_{M+1} peaks over time (after time t) can be expressed by Equations (8) and (9) [10].

$$I_M(t) = I_M(0) \cdot e^{-k_\varphi t} \tag{8}$$

$$I_{M+1}(t) = I_{M+1}(0) \cdot e^{-k_\varphi t} + I_M(0)\left[1 - e^{-k_\varphi t}\right] \tag{9}$$
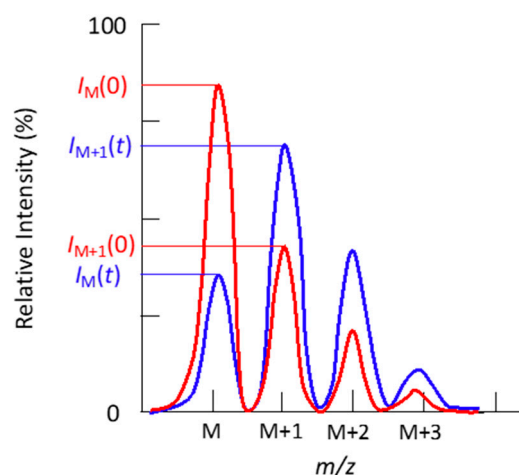

Figure 4. The change in the cluster of isotopic peaks before (red) and after (blue) HDX reaction.

Dividing Equation (9) by Equation (8) yields

$$\frac{I_{M+1}(t)}{I_M(t)} = \frac{I_{M+1}(0)}{I_M(0)} + e^{k_\varphi t} - 1 \tag{10}$$

Since $I_{M+1}(0)/I_M(0)$ and $I_{M+1}(t)/I_M(t)$ represent the ratios between I_M and I_{M+1} peaks before (time = 0) and after (time = t) HDX reaction, respectively, defining these ratios as $R(0)$ and $R(t)$, Equation (10) can be expressed as follows:

$$R(t) = R(0) + e^{k_\varphi t} - 1 \tag{11}$$

Taking the logarithm on both sides of Equation (11) and rearranging it yields the following equation:

$$\ln[1 + R(t) - R(0)] = k_\varphi t \tag{12}$$

This equation expresses the linear relationship between $\ln[1 + R(t) - R(0)]$ and time t with the slope as k_φ. Therefore, k_φ can be calculated using the following equation.

$$k_\varphi = \ln[1 + R(t) - R(0)]/t \tag{13}$$

Once the value of k_φ is obtained, it is possible to estimate pK_a and k_φ^{max} values graphically using a non-linear least-square fit program (see Figure 3).

In the HDX experiments using a mixture of H_2O and D_2O as solvent, Equations (8) and (9) should be modified to include the fraction of D_2O content in the solvent, $p = [D_2O]/([D_2O] + [H_2O])$, as a factor limiting the maximum increase in mass by p Da. That is, transforming Equations (8) and (9) to

$$I_M(t) = I_M(0) - \left[I_M(0)\left(1 - e^{-k_\varphi t}\right)p\right] \tag{14}$$

and

$$I_{\text{M+1}}(t) = \left\{ I_{\text{M+1}}(0) - \left[I_{\text{M+1}}(0)\left(1 - e^{-k_\varphi t}\right)p \right] \right\} + \left[I_{\text{M}}(0)\left(1 - e^{-k_\varphi t}\right)p \right] \quad (15)$$

From Equations (14) and (15), the following equation for obtaining k_φ is derived [24].

$$k_\varphi = -\ln\left\{ 1 - \left[\frac{\{R(t) - R(0)\}}{1 + R(t) - R(0)} \right]\frac{1}{p} \right\}/t \quad (16)$$

Equation (13) is considered a special case of Equation (15), in which $p = 1$ (100% D_2O). Equation (16) is particularly useful when a mixed solvent of D_2O and H_2O is used in the HDX reaction.

It is also possible to obtain k_φ by employing the shift in weighted average mass $M_{wt,av}(t)$ in the range $M_{wt,av}(0) \leq M_{wt,av}(t) \leq M_{wt,av}(0) + 1$ or $0 \leq \Delta M_{wt,av}(t) \leq 1$ [$\Delta M_{wt,av}(t) = M_{wt,av}(t) - M_{wt,av}(0)$] [25,26]. The values $M_{wt,av}(0)$ at $t = 0$ and $M_{wt,av}(t)$ at time t can be calculated from the isotopomer distribution of a given peptide peak. Since the HDX reaction follows pseudo-first-order kinetics, the shift in weighted average mass over time (t) can be expressed as follows:

$$\ln[1 - \Delta M_{wt,av}(t)] = -k_\varphi t \quad (17)$$

Therefore, k_φ can be calculated using the following equation.

$$k_\varphi = -\ln[1 - \Delta M_{wt,av}(t)]/t \quad (18)$$

Equation (17) can incorporate the factor p (the fraction of D_2O content in the reaction) by replacing the maximum $M_{wt,av}(t) = 1$ with p, as follows:

$$\ln[p - \Delta M_{wt,av}(t)] = -k_\varphi t \quad (19)$$

Thus, k_φ can be calculated using the following equation.

$$k_\varphi = -\ln[p - \Delta M_{wt,av}(t)]/t \quad (20)$$

When the isotopic peak envelope of a molecular ion is obtained with a good signal-to-noise (S/N) ratio and without any interference peaks, Equations (13) and (18) can be reliably used without any preference. Regardless of the choice, it is essential to exercise extra caution for possible errors caused by low S/N spectra or the presence of interference peaks. Elferich and co-workers demonstrated that accurate calculation of deuterium incorporation can be achieved even with low S/N data by fitting the observed isotopic distribution with a linear combination of theoretical isotopic distributions of non-exchanged and fully exchanged peptides [27]. Another consideration to keep in mind when analyzing HDX data is that in His-HDX experiments, the protein samples are typically incubated for an extended period (more than 2 days). Therefore, special caution should be exercised when analyzing the mass spectrometry data, as deamidation of Asn or Gln residues could occur, resulting in an additional increase in mass of 1 Da. Since liquid chromatography is likely to separate the original peptide and its deamidated forms, LC-MS would be less susceptible to this problem than MALDI-MS.

2.3.3. Relationship between pK_a and k_φ^{max}

The maximum hydrogen–deuterium exchange (HDX) rates, represented as intrinsic k_φ^{max} ($^i k_\varphi^{\text{max}}$), for C-2 hydrogens fully exposed to the solvent vary based on their pK_a values, as illustrated in Figure 5. Consequently, for a precise quantitative interpretation of the experimentally obtained k_φ^{max} value for a particular His residue, it is essential to be aware of the $^i k_\varphi^{\text{max}}$ value of an imidazole group sharing the same pK_a value as the given imidazole group.
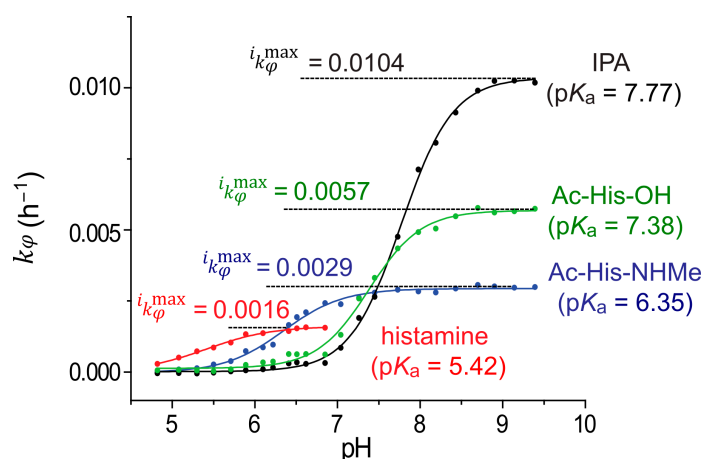
Figure 5. pK_a dependence of the intrinsic maximum HDX rates, $^i k_\varphi^{\max}$. pH dependence of the HDX rate, k_φ, for the imidazole groups in histamine (red), Ac-His-NHMe (blue), Ac-His-OH (green) and IPA (1H-imidazole-5-propanoic acid, black) is shown. Experimentally obtained pK_a values and intrinsic maximum HDX rates, $^i k_\varphi^{max}$, for the four imidazole derivatives are shown. This figure was modified from Figure 2 in Ref. [28].

The maximum exchange rates of C-2 hydrogens, which are fully exposed to the solvent—defined as intrinsic maximum HDX rates, $^i k_\varphi^{\max}$—differ depending on their pK_a values, as shown in Figure 5 [28]. Therefore, to quantitatively interpret the experimentally obtained $k_\varphi^{\max}$ value for a specific His residue, it is necessary to know the $^i k_\varphi^{\max}$ value of an imidazole group with the same pK_a value as the given imidazole group.

As shown in Scheme 2, the hydrogen exchange reaction of imidazole C-2 position is based on a base-catalyzed reaction to which a linear free-energy relationship known as the Brønsted equation is applicable, as follows:

$$\log k = \alpha \cdot \mathrm{p}Ka + \beta \tag{21}$$

Matsuo and colleagues determined factor α to be –0.7 using the hydrogen–tritium exchange (HTX) method, with several model compounds containing an imidazole group fully exposed to water to correlate $k_\varphi^{\max}$ with accessibility of the imidazole group to the solvent [29–31]. This linear relation still proved useful in the HDX method applied to His residues in RNase A [20].

Miyagi and colleagues also determined factor α and β using four imidazole derivatives, shown in Figure 5, resulting in the following equation [28]:

$$\log {}^i k_\varphi^{max} = 0.316(\mathrm{p}K_a - 7) + (0.057T - 3.747) \tag{22}$$

This equation involves temperature T in the Celsius scale for the sake of convenience in establishing the relationship between $^i k_\varphi^{\max}$ and pK_a values at any temperature. The inversion of the logarithm function yields the $^i k_\varphi^{max}$ value. By utilizing the protection factor (PF), defined as follows, one can quantitatively estimate the solvent accessibility of His residues in proteins [32].

$$PF = \frac{{}^i k_\varphi^{max}}{k_\varphi^{\max}} \tag{23}$$

In this context, a smaller PF value corresponds to higher solvent accessibility, with a value of 1 indicating complete exposure to the bulk solvent.

3. Experimental Workflow of His-HDX-MS Experiment

The general workflow of the His-HDX-MS experiment is depicted in Figure 6. First, the protein(s) is/are incubated in buffers made with D$_2$O at various pD values for 2–3 days

to allow His residues to incorporate a deuterium atom. After incubation, the reaction is quenched by adding formic acid to adjust the solution's pH to below 4. Then, the protein is digested in H_2O, during which all the deuterium atoms incorporated into amide (Asn/Gln/backbone), OH (Ser/Thr), NH_2 (Lys/N-terminal), COOH (Asp/Glu/C-terminal), indole NH (Trp), ε-, η_1- and η_2-NH (Arg), SH (Cys) and imidazole NH (His) exchange back to protium almost instantaneously (<1 s at physiological pH at 37 °C, if not protected from access to H_2O) [33], leaving the deuterium atom at the imidazole C-2 position (C-2 D) as the only deuterium remaining in the protein. To minimize the extent of C-2 D to C-2 H back-exchange reaction, the digestion is often completed within 1–2 h using immobilized proteases at pH 7–8. However, even when digesting proteins for 16 h at 37 °C, only approximately 16% of C-2 D is exchanged back to C-2 H based on the rate constant for the back-exchange reaction ($k = 0.011 \text{ h}^{-1}$) [34]. After digestion, the digests are analyzed by LC-MS/MS. The back-exchange reaction during a typical LC-MS analysis under acidic pH condition is negligible, since essentially no C-2 D to C-2 H reaction occurs below pH 4 [10]. The mass spectrometry data obtained are then analyzed to obtain the pseudo-first-order rate constant (k_φ), as discussed above. The rate of HDX reaction (k_φ) as a function of pD yields a sigmoidal curve. The rate profile provides two useful parameters, which indicate the local environment of the given imidazole group in a protein. The first is the pK_a of the imidazole N–H group, which coincides with the inflection point of the sigmoidal curve. The second is the maximum pseudo-first-order rate constant, $k_\varphi^{\max}$, which corresponds to the upper plateau of the sigmoidal curve and indicates the solvent accessibility of the imidazole group expressed as a PF value, as discussed above. Based on the $k_\varphi^{\max}$ value, the half-life of the HDX rate can also be calculated using the following equation:

$$t_{1/2} = \ln 2 / k_\varphi^{\max} \tag{24}$$
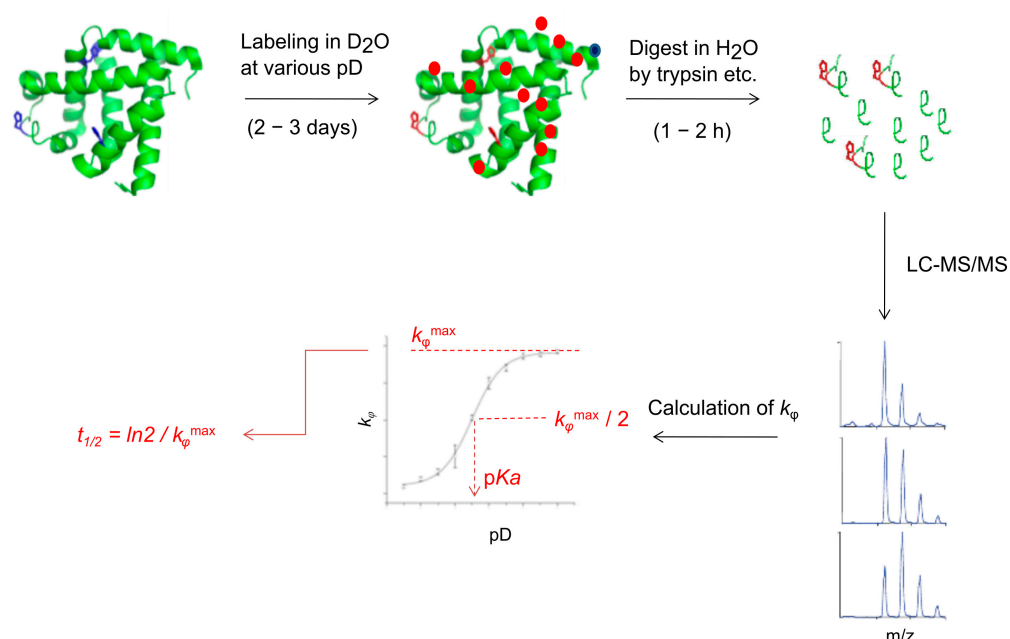
Figure 6. General workflow of His-HDX-MS experiments.

The pH titration experiment detailed above represents a fully executed His-HDX-MS study, yielding both pK_a and $k_\varphi^{\max}$ values. Nonetheless, a simpler approach—such as measuring the HDX rates of His residues in unliganded and ligand-bound proteins at a fixed pH—can still offer significant insights into understanding the structural changes in proteins. However, it is crucial to highlight that the derived rate constant $k\varphi$ is distinct from $k_\varphi^{\max}$. While $k_\varphi^{\max}$ allows for a quantitative description of solvent accessibility, the rate constant $k\varphi$ simply represents a specific rate at the measured pH.

It should be noted, however, that obtaining residue-specific k_φ or $k_\varphi^{\max}$ values is not straightforward when multiple His residues exist in a peptide. This complexity arises because the precursor ion of the peptide reflects the combined HDX reactions from multiple His residues. To address this, careful selection of the protease(s) is necessary during protein digestion to ensure the production of peptides containing only a single His residue. An alternative way of tackling this issue is to use tandem mass spectrometry techniques. Wimalasena and colleagues used the collision-induced dissociation (CID) technique for a peptide with three His residues. They successfully determined the HDX rates of these three His residues using fragment ions containing only one of the three His residues [35]. Elferich and colleagues employed the electron-transfer dissociation (ETD) technique to fragment the furin propeptide (approximately 9200 Da) and successfully determined the pK_a and $k_\varphi^{\max}$ values of five His residues without using any proteases [27]. The employment of such peptide fragmentation techniques can significantly augment the effectiveness of His-HDX-MS, particularly for proteins with multiple His residues in a short sequence range. These examples illustrate the absence of C2-deuterium migration to other peptide regions during CID or ETD. This stands in contrast to amide-HDX-MS, where notable scrambling of amide-deuterons occurs during CID [36,37], albeit to a much smaller extent during ETD [38–40] or ultraviolet photodissociation (UVPD) [41,42].

4. Strengths and Limitations of His-HDX-MS

A variety of techniques are available for characterizing protein structures and dynamics. X-ray crystallography, NMR spectroscopy and cryo-electron microscopy are commonly chosen methods for determining protein structures at atomic resolution. Additionally, techniques such as circular dichroism spectroscopy, fluorescence spectroscopy and mass spectrometry are primarily employed to characterize the dynamic properties of proteins, focusing on backbone and side-chain mobilities. The strengths of mass spectrometry include (1) straightforward assignment of molecular ions to protein sequences, (2) high detection sensitivity and (3) no limitation on the sizes of proteins. Thus, compared to NMR-based methods, His-HDX-MS, which is based on mass spectrometry, provides a more straightforward assignment of pK_a values to individual His residues, requiring a significantly smaller quantity of protein.

The most commonly used mass spectrometry technique when studying protein structure and dynamics is amide-HDX-MS [43–45], which monitors the HDX rates of the backbone amide. The major technical challenge of amide-HDX-MS is the fast back exchange from deuterium to proton, which can occur during protein digestion and mass spectrometry analysis. This reaction is fast; the half-life for the back-exchange reaction is about 1 h at pH 2.5 and at 0 °C [46,47], necessitating completion of the digestion of proteins at acidic pH and analysis of the resulting peptides with LC-MS/MS in approximately 1 h. In contrast, the rate of His-HDX is much slower ($t_{1/2}$ = 1.9 days at 37 °C) [34], allowing for relatively long protein digestion at physiological pH at 37 °C using proteases, which work at physiological pH. Additionally, in amide-HDX-MS, the LC-MS separation of peptides is conducted at low temperatures (close to 0 °C) to avoid back exchange. However, since essentially no back-exchange reaction occurs below pH 4 [10], in His-HDX-MS, a long chromatographic separation of peptides at a higher temperature can be employed to enhance the efficiency of peptide separation [48,49].

The major limitations of His-HDX compared to amide-HDX-MS are twofold: (1) the technique relies on the presence of His residues and (2) requires a long incubation time (>48 h at 37 °C). The occurrence of histidine residues in human proteins is 2.6%, which equates to 2–3 His residues in every 100 amino acid residues [50]. Therefore, His-HDX-MS is limited to probing the local electrostatic environment and solvent accessibility of His residues. Another limitation is the requirement for a long incubation time. Thus, this technique is not suitable for proteins, which are not stable.

5. Applications of His-HDX-MS and the Interpretation of His-HDX-MS Data

5.1. Applications of His-HDX-MS

The primary application of His-HDX-MS is in determining the pK_a values and solvent accessibilities of histidine (His) residues within proteins. In a study by Miyagi and colleagues, changes in the pK_a and k_φ^{max} values of five histidine residues in dihydrofolate reductase (DHFR) upon ligand binding were investigated [24]. The findings underscored the high sensitivity of pK_a and k_φ^{max} values to changes in the electrostatic environment and solvent accessibilities of these histidine residues, respectively. A study by Hayashi and colleagues on RNase A in the presence and absence of its ligand—cytidine 3′-monophosphate (3′-CMP)—also provided in-depth insights into the micro-environment of three His residues, including possible hydrogen bonding networks [26]. Consequently, the determination of pK_a and k_φ^{max} values could provide valuable insights into the micro-environment of His residues, facilitating a better understanding of their roles in protein functions.

Elferich and colleagues determined the pKa values of the conserved His residue in the propeptides of furin and proprotein convertase 1/3 to be 6.0 and 5.6, respectively [27]. The result was consistent with the different activation pHs of these proteins (furin: pH 6.5 and proprotein convertase 1/3: pH 5.5), indicating that protonation of the conserved His residue triggers the activation processes of these proteins. Miyahara and colleagues investigated the susceptibility of monoclonal antibodies—adalimumab and rituximab—to photo-oxidation and found that photo-oxidation occurs preferentially in His residues with low pK_a values [51], indicating that the unprotonated imidazole ring is more susceptible to oxidation. Therefore, storing antibodies under acidic conditions could prevent oxidation. The two studies underscore the fact that assessing the protonation states of His residues could provide insights into the pH-dependent conformational changes in proteins or susceptibility to photo-oxidation.

His-HDX-MS has been employed to study structural changes in the G-protein-coupled receptor rhodopsin in its apo and ligand-bound forms in the native membrane prepared from bovine retina [52]. This technique has also been used to study the activation mechanism of protease-activated receptor 4, another G-protein-coupled receptor [53]. These studies demonstrated that His-HDX-MS can be applied to membrane proteins without much difficulty, unlike amide-HDX-MS, which requires the digestion and analysis of protein samples within a short period of time (<2 h) due to the fast back-exchange reaction of amide deuteron to proton.

Surewicz's group employed His-HDX-MS in conjunction with amide-HDX-MS to study the structures of different forms of prion proteins [54–57]. These studies showcased the complementary nature of His-HDX-MS and amide-HDX-MS. The former delves into the micro-environment of His residues, while the latter unveils the conformational flexibility of backbone amides throughout the structure. Therefore, it is recommended to leverage both techniques when technical expertise is available.

His-HDX-MS has also served as the basis for measuring the thermodynamic stability of proteins. Fitzgerald's group pioneered the development of a method for assessing the thermodynamic stability of protein–ligand and protein–protein interactions [25,58]. In this approach, proteins are incubated in a D_2O buffer with varying concentrations of a protein denaturant (e.g., guanidine hydrochloride), and proteins are then digested and analyzed by LC-MS/MS. The results provide protein-denaturant concentration-dependent HDX rates of His residues from which the free-energy change ($\Delta G°$) in protein denaturation can be estimated. This approach has also been employed in monitoring the thermodynamic stability changes in anthrax protective antigen upon binding to its receptor—capillary morphogenesis protein-2 (CMG2)—revealing that the protective antigen is stabilized by CMG-2 [59]. Additionally, the approach has been utilized to identify protein–drug interactions [34]. Despite the availability of various techniques for measuring protein stability or protein folding/unfolding, the strength of His-HDX-MS lies in its applicability to complex protein mixtures.

His-HDX-MS has also been utilized by Cebo and colleagues to identify phosphorylated His residues in proteins [60]. They verified that phosphorylation dramatically slows the rate of C-2 hydrogen HDX, thereby allowing the detection of phosphorylated His residues. Vachet's group showed that the HDX rates of metal-bound His residues are significantly slower than their free forms [61,62] and demonstrated that His-HDX-MS can be used to identify metal-bound His residues.

5.2. Implication of pK$_a$ and Kinetic Parameters in the Context of the Function of His Residues in Proteins

5.2.1. pK$_a$ Values and Enzyme Catalysis

The pK$_a$ values of His residues can shift appreciably due to interactions with the surrounding functional groups in proteins or substrates. It is widely acknowledged that adjacent groups contributing to higher electron density in the imidazole ring, such as $RCOO^-$, RO^-, RS^-, elevate the pK$_a$ of the imidazole ring, while neighboring groups, which diminish the electron density of the imidazole ring, such as RNH_3^+, $GdnH^+$, ImH^+, lead to lowering the pK$_a$ of the imidazole ring [63]. There are many His residues reported to have exhibited highly deviant pK$_a$ values from the well-acknowledged range of 6–7, suggesting the existence of interactions with ionizable functional groups directly or via hydrogen bond networks [2,64]. The relationship between the acid-base properties of His residues and enzyme catalysis was first noted for catalytic residues His12 and His119 in RNase A in 1961 [65]. Since this study, many researchers have attempted to measure the pK$_a$ values of these residues using ^{1}H NMR [5,8,9,12,14,17,66,67], His-HTX [15,30,68] and His-HDX-MS [10,26]. For example, the pK$_a$ value of His12 changes from 5.8 in the free enzyme to 7.1 in the complex with 3′-cytidine monophosphate (3′-CMP) [26]. A similar but less significant alkaline shift in pK$_a$ from 6.3 to 7.0 was observed for His119 [26]. These results suggest that His12 and His119 cooperatively act as an acid and a base in their reversed roles before and after the binding of 3′-CMP, which is in consistent with the most classic catalytic mechanism [65]. A recent perspective on the RNase A reaction mechanism has been summerized by Raines and colleagues [69,70]. Thus, measuring the pK$_a$ values of catalytic His residues in enzymes may provide some insights for understanding their catalytic mechanisms.

5.2.2. Double Sigmoidal Titration Curve: pK$_a$ Values in His HDX and NMR

Double sigmoidal curves could be observed for His imidazole groups, which are in close proximity to ionizable groups. In the cases of RNase T$_1$ and RNase St, several His residues exhibited double sigmoidal titration curves both in HTX and NMR titration experiments [29,31]. A double sigmoidal titration curve in the plot in Figure 7 infers the existence of a charged group near a His residue. Suppose a pair of Lys and His residues are mutually interacting with each other in equilibrium, and their pK$_a$ values differ by more than two pH units [30,71]. In an NMR titration experiment, the inflection points at lower and higher pH values are considered to correspond to the pKa of the imidazole group of His residues and the amino group of Lys, respectively. However, in the His-HDX experiment, both inflection points reflect the acid-base equilibria of His residues influenced by the protonation/deprotonation of the Lys amino group. This is because the HDX reaction proceeds solely through the equilibrium involving the imidazolium cation (Im·H$^+$) of the His residue (see Scheme 2). Consequently, the HDX microscopic dissociation constants obtained through the His-HDX experiment—namely pK$_1$ and pK$_4$ in Figure 7—reflect the dissociations of the imidazolium group when Lys is protonated (equilibrium between systems I and II) and deprotonated (equilibrium between III and IV), respectively (refer to Scheme 3). Although the dissociation constants K_2 and K_3 are not measurable by His-HDX-MS, they can be calculated, if necessary, from the macroscopic dissociation constants obtained from the double sigmoidal curve of the NMR titration experiment, as described by Rabenstein and Sayer [72]. Thus, double sigmoidal titration

curves provide two well-defined sets of microscopic pK_a and $k_\varphi^{\max}$ values reflecting the ionizable group(s) around His residues.
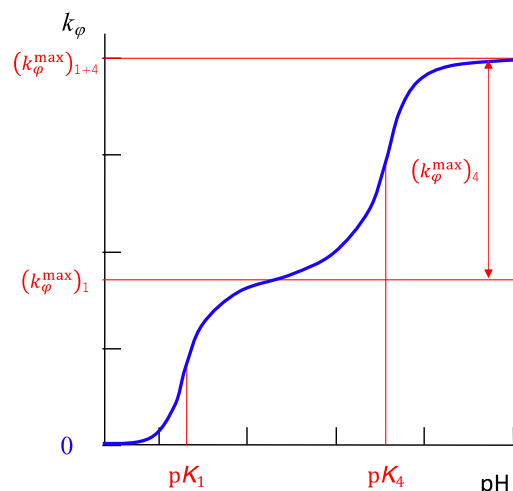

Figure 7. Sketch of a double sigmoidal titration curve expected to be obtained from the HDX experiment on a His residue influenced by the ionization state of the amino group of a Lys residue in neutral (Lys) and protonated (Lys+) forms. The dissociation constants pK_1 and pK_4 reflect the dissociations of the imidazolium group when Lys is protonated and deprotonated, respectively. Under these conditions, the rate constants $\left(k_\varphi^{\max}\right)_1$ and $\left(k_\varphi^{\max}\right)_4$ correspond to the $k_\varphi^{\max}$ values of the HDX reaction occurring for protonated and neutral forms of Lys, respectively. Hence, the total HDX rate constant, $\left(k_\varphi^{\max}\right)_{1+4}$ is the sum of $\left(k_\varphi^{\max}\right)_1$ and $\left(k_\varphi^{\max}\right)_4$.
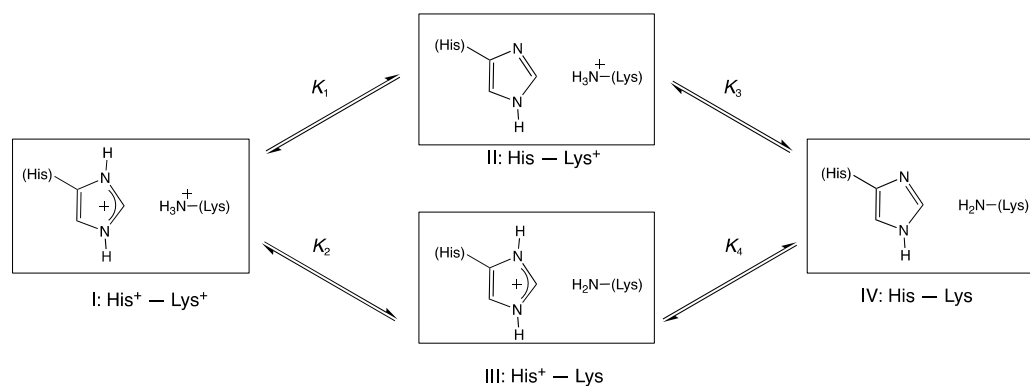
Scheme 3. The microscopic dissociation equilibria of systems consisting of His and Lys in their protonated and non-protonated forms. In System I, both the imidazole group of His and the ε-amino group of Lys are protonated, designated as His+ and Lys+. In System II, the imidazole group of His is deprotonated, while the ε-amino group of Lys is protonated (His and Lys+). In System III, the imidazole group of His is protonated, while the ε-amino group of Lys is deprotonated (His+ and Lys). In System IV, both the imidazole group of His and the ε-amino group of Lys are deprotonated (His and Lys). The arrows indicate the reversibility among the systems. It is assumed that these two residues are not necessarily exchanging proton directly but are sufficiently close to interact electrostatically. The His+ form in Systems I and III serves as the sole species, which can react with the OD$^-$ ion to proceed to the exchange of the C-2 proton (see Scheme 2).

5.3. His HDX Rate and Solvent Accessibility as Factors Reflecting Protein Structure

The PF values for the His imidazole groups defined in Equation (23) have been demonstrated to correlate well with the solvent-accessible surface area (ASA) calculated from the crystal structures of proteins, as discussed in Section 2.3. Thus, PF values are a useful indicator for predicting the solvent accessibility of His residues in proteins. In the

case of an enzyme DHFR in apo and its complex with folate and NADP$^+$, the PF values determined for four out of five His residues had a fairly good correlation with ASA, as shown in Figure 8 [28]. Notable exceptions include the anomalous shift in ASA-PF data obtained for His149, which appeared to be shielded from access to the solvent in the apo form more than in the complex, given the approximately two-fold decrease in ASA value in the apo form. However, the PF values of both forms were almost indistinguishable. This inconsistency could possibly be attributed to the difficulty in calculating ASA based on the PDB data of apo-DHFR (5DFR), in which the local structure involving His149 (His149(a) in Figure 8) in the G-H loop fluctuates minutely between "open", "closed" and "occluded" conformations [73,74]. In contrast, the most appreciable deviation of the PF value from ASA was observed for His114 in DHFR complexed with folate and NADP$^+$. According to the X-ray structure of the DHFR–folate–NADP$^+$ complex (PDB ID: 1RX2) [74], the involvement of His114, Glu154 and Ser135 in a network of hydrogen bonds could be the main reason for suppression of the HDX reaction of His114 in comparison with the almost unrestrained condition of this residue in the apo form of the enzyme (PDB ID: 5DFR). Thus, the PF–ASA plot may exhibit His residues with unusual structural features beyond solvent accessibility.
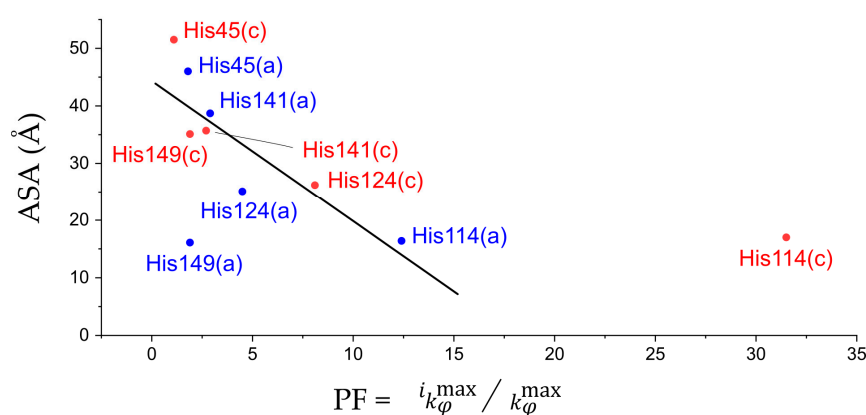

Figure 8. PF versus ASA plot for five His residues of *E. coli* DHFR. Data points plotted in blue denote His residues in apo-DHFR (a), and those plotted in red denote His residues in complex with folate and NADP$^+$ (c). This plot was produced using data contained in Table 2 in Ref. [28]. The linear regression line was established by excluding the data points corresponding to His149(a) and His114(c), leading to an R-squared value of 0.79.

His residues with extremely low $k_\varphi^{\max}$ values are generally considered to be almost completely shielded from access to water or deeply "buried" within the protein structure, with the exception of His residues coordinating with metal ions. Indeed, the reaction rate of His HDX depends proportionally on the concentration of the deuteroxide ion, $[OD^-]$, in bulk water, as shown in Equation (4). However, it is not rare to encounter a fairly high value of ASA being calculated for His residues for which the HDX rates are unusually slow [3]. One notable example includes His25 in FK506 binding protein. The ASA value of His25 in this protein is quite high (52.6% of fully exposed residue). However, the kinetic constants could not be determined under ^{1}H NMR titration, likely due to its exceptionally low pK_a value [3,75]. The challenge in obtaining a sigmoidal curve is anticipated in Equation (22), explaining that the intrinsic HDX reaction rate, $^i k_\varphi^{\max}$, decreases logarithmically with the reduction in pK_a value.

Table 1 lists several His residues—including His25 in FK506 binding protein—in which the determination of pK_a values was challenging due to extremely slow HDX rates and the absence of substantial pH dependency in titration data. His48 in RNase A serves as another example, illustrating a low pK_a value accompanied by an exceptionally slow HDX rate. Within the hydrogen bond network, as revealed by the X-ray structure of RNase A (PDB ID: 1RPH), the imidazole group of His48 in β-strand 1 is situated between the hydroxy group of Thr82 in β-strand 1 and the amide carbonyl group of Asp14 in loop 1, as

depicted in Scheme 4. Within this hydrogen bond network, the imidazole group of His48 is predominantly found in the neutral form, rendering it incapable of participating in HDX reaction [26]. As a result, the HDX rate is significantly slower than the rate estimated by its ASA. Thus, the relationship between PF and ASA values is often not straightforward and requires careful interpretation. However, it could include valuable information, which cannot be obtained using other structural biology techniques.

Table 1. Slow HDX rates of His residues in proteins.

Protein	Positions of His Residues	Protein Data Bank ID	Kinetic Data/Method [Reference]
RNase A	48	1RPH	nt [a]/NMR [17,76], $t_{1/2} > 58$ days/HTX [15], $t_{1/2} = 46$ days/HDX [10]
FK506 binding protein	25	1FKJ	nt ($pK_a < 3.6$)/NMR [75]
Cyclophilin	54	6FK1	nt ($pK_a < 4.2$)/NMR [75]
Phosphatidylinositol-specific phospholipase C	61, 81	3PTD	nt ($pK_a < 3$)/NMR [77]
G-protein-coupled receptor rhodopsin	152, 211, 279	3CAP	$t_{1/2} > 50$ h/HDX [52] [b]
Protective antigen—Capillary morphogenesis protein 2	253, 336, 616	3Q8B 1T6B (complex)	$t_{1/2} > 10$ days/HDX [59] [c]
Protease-activated receptor 4	159, 269	Not available	$t_{1/2} > 50$ days/HDX [53] [d]

[a] nt: Not titratable. [b] Determined at pH 8.0. [c] Determined at pH 9.0. [d] Determined at pH 7.5.
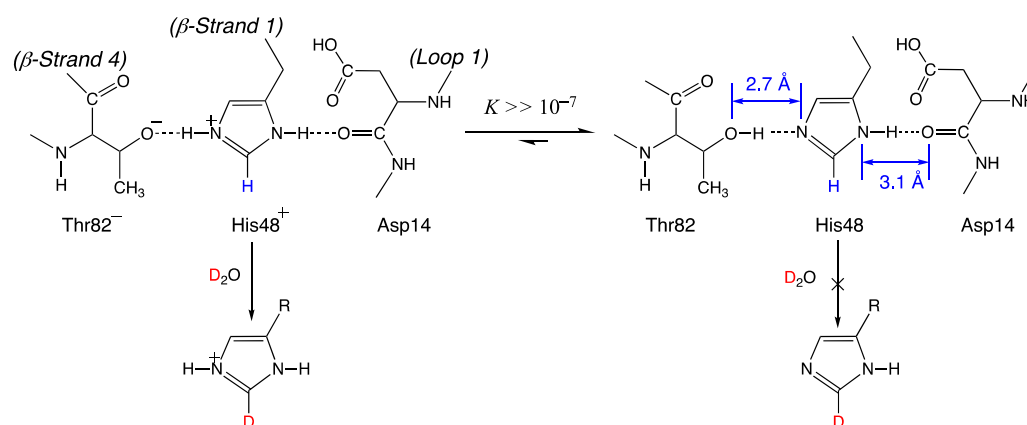
Scheme 4. A possible mechanism of the extremely slow C-2 HDX reaction in His48. The network of hydrogen bonds connecting Thr82, His48 and Asp14 virtually restricts the imidazole group of His48 to the electrically neutral state due to the overwhelmingly lower acidity of the hydroxy group ($pK_a > 14$) than the imidazolium group. The C-2 proton (blue) is replaced by deuteron (red) in this reaction (see also Scheme 2). Note that HDX reaction can occur only through the imidazolium cation, which can populate only marginally in this situation. PDB code 1RPH was used to create this scheme.

6. Conclusions

In summary, His-HDX-MS offers valuable insights into two key properties of histidine imidazole groups within proteins. First, it provides information on pK_a values, reflecting the electrostatic environment surrounding a specific His imidazole group. Second, it can measure the His imidazole group's HDX rate, which serves as an indicator of solvent accessibility, conformational stability and fluctuation. These parameters are instrumental in understanding enzyme mechanisms, ligand-induced conformational changes in proteins and various other crucial processes. Although there remains a challenge in elaborating on the mechanism of enhancing or attenuating His HDX rate by the environment—influencing the reactivity of the imidazolium group through hydrogen bond

or electrostatic interaction—we believe there are ample opportunities for this technique to prove highly beneficial in the field of structural biology research.

His-HDX-MS is well suited to analyzing complex protein mixtures, such as cell lysates. Owing to the slow back exchange of imidazole C-2 D to C-2 H, proteases with strict substrate specificities (e.g., trypsin) can be used, which provides higher peptide discrimination power in peptide identification. Additionally, slow back exchange allows the employment of long chromatographic separation in the LC-MS/MS analysis in order to enhance peptide separation. Additionally, a highly efficient histidine-containing peptide enrichment method is available [34], which significantly simplifies proteome samples and enhances the identification of His-containing peptides. For these reasons, His-HDX-MS should be applied more to proteome-scale samples in the near future, as also noted by Courouble and colleagues in their recent review paper [44]. Lastly, there is currently no computational tool available for automating the data analysis step. The availability of such software will encourage scientists in the field to use this method.

Author Contributions: M.M. initiated the plan for the article; T.N. wrote the first draft. Both authors contributed equally to the final version. All authors have read and agreed to the published version of the manuscript.

Institutional Review Board Statement: Not applicable.

Informed Consent Statement: Not applicable.

Data Availability Statement: Not applicable.

Conflicts of Interest: The authors declare no conflicts of interest.

References

1. Nomenclature and Symbolism for Amino Acids and Peptides (Recommendations 1983). *Pure Appl. Chem.* **1984**, *56*, 595–624. [CrossRef]
2. Antosiewicz, J.; Mccammon, J.A.; Gilson, M.K. The Determinants of pKas in Proteins. *Biochemistry* **1996**, *35*, 7819–7833. [CrossRef] [PubMed]
3. Edgcomb, S.P.; Murphy, K.P. Variability in the pKa of Histidine Side-Chains Correlates with Burial within Proteins. *Proteins Struct. Funct. Genet.* **2002**, *49*, 1–6. [CrossRef] [PubMed]
4. Couch, V.; Stuchebrukhov, A. Histidine in Continuum Electrostatics Protonation State Calculations. *Proteins Struct. Funct. Bioinforma.* **2011**, *79*, 3410–3419. [CrossRef] [PubMed]
5. Markley, J.L. Observation of Histidine Residues in Proteins by Nuclear Magnetic Resonance Spectroscopy. *Acc. Chem. Res.* **1975**, *8*, 70–80. [CrossRef]
6. Markley, J.L.; Ibañez, I.B. Zymogen Activation in Serine Proteinases. Proton Magnetic Resonance pH Titration Studies of the Two Histidines of Bovine Chymotrypsinogen A and Chymotrypsin Aalpha. *Biochemistry* **1978**, *17*, 4627–4640. [CrossRef] [PubMed]
7. Ash, E.L.; Sudmeier, J.L.; De Fabo, E.C.; Bachovchin, W.W. A Low-Barrier Hydrogen Bond in the Catalytic Triad of Serine Proteases? Theory versus Experiment. *Science* **1997**, *278*, 1128–1132. [CrossRef]
8. Hansen, A.L.; Kay, L.E. Measurement of Histidine pKa Values and Tautomer Populations in Invisible Protein States. *Proc. Natl. Acad. Sci. USA* **2014**, *111*, E1705–E1712. [CrossRef]
9. Meadows, D.H.; Markley, J.L.; Cohen, J.S.; Jardetzky, O. Nuclear Magnetic Resonance Studies of the Structure and Binding Sites of Enzymes. I. Histidine Residues. *Proc. Natl. Acad. Sci. USA* **1967**, *58*, 1307–1313. [CrossRef]
10. Miyagi, M.; Nakazawa, T. Determination of pKa Values of Individual Histidine Residues in Proteins Using Mass Spectrometry. *Anal. Chem.* **2008**, *80*, 6481–6487. [CrossRef]
11. Wüthrich, K. *NMR of Proteins and Nucleic Acids*; The George Fisher Baker non-resident lectureship in chemistry at Cornell University; Wiley: New York, NY, USA, 1986; ISBN 978-0-471-82893-8.
12. Meadows, D.H.; Jardetzky, O.; Epand, R.M.; Ruterjans, H.H.; Scheraga, H.A. Assignment of the Histidine Peaks in the Nuclear Magnetic Resonance Spectrum of Ribonuclease. *Proc. Natl. Acad. Sci. USA* **1968**, *60*, 766–772. [CrossRef] [PubMed]

13. Shimahara, H.; Yoshida, T.; Shibata, Y.; Shimizu, M.; Kyogoku, Y.; Sakiyama, F.; Nakazawa, T.; Tate, S.; Ohki, S.Y.; Kato, T.; et al. Tautomerism of Histidine 64 Associated with Proton Transfer in Catalysis of Carbonic Anhydrase. *J. Biol. Chem.* **2007**, *282*, 9646–9656. [CrossRef] [PubMed]

14. Matsuo, H.; Ohe, M.; Sakiyama, F.; Narita, K. A New Approach to the Determination of pKa's of Histidine Residues in Proteins. *J. Biochem.* **1972**, *72*, 1057–1060. [CrossRef] [PubMed]

15. Ohe, M.; Matsuo, H.; Sakiyama, F.; Narita, K. Determination of pKa's of Individual Histidine Residues in Pancreatic Ribonuclease by Hydrogen-Tritium Exchange. *J. Biochem.* **1974**, *75*, 1197–1200. [CrossRef] [PubMed]

16. Fersht, A. The pH Dependence of Enzyme Catalysis. In *Structure and Mechanism in Protein Science. A Guide to Enzyme Catalysis and Protein Folding*; Fersht, A., Ed.; World Scientific Publishing Co., Pte. Ltd.: Singapore, 2017; pp. 169–190.

17. Markley, J.L. Correlation Proton Magnetic Resonance Studies at 250 MHz of Bovine Pancreatic Ribonuclease. I. Reinvestigation of the Histidine Peak Assignments. *Biochemistry* **1975**, *14*, 3546–3554. [CrossRef] [PubMed]

18. Olofson, R.A.; Thompson, W.R.; Michelman, J.S. Heterocyclic Nitrogen Ylides. *J. Am. Chem. Soc.* **1964**, *86*, 1865–1866. [CrossRef]

19. Harris, T.M.; Randall, J.C. Deuterium Exchange Reactions at the C2-Position of Imidazoles. *Chem. Ind.* **1965**, *41*, 1728–1729.

20. Vaughan, J.D.; Mughrabi, Z.E.; Wu, C. The Kinetics of Deuteration of Imidazole. *J. Org. Chem.* **1970**, *35*, 1141–1145. [CrossRef]

21. Bradbury, J.H.; Chapman, B.E.; Pellegrino, F.A. Hydrogen-Deuterium Exchange Kinetics of the C-2 Protons of Imidazole and Histidine Compounds. *J. Am. Chem. Soc.* **1973**, *95*, 6139–6140. [CrossRef]

22. Amyes, T.L.; Diver, S.T.; Richard, J.P.; Rivas, F.M.; Toth, K. Formation and Stability of N-Heterocyclic Carbenes in Water: The Carbon Acid pKa of Imidazolium Cations in Aqueous Solution. *J. Am. Chem. Soc.* **2004**, *126*, 4366–4374. [CrossRef]

23. Covington, A.K.; Robinson, R.A.; Bates, R.G. The Ionization Constant of Deuterium Oxide from 5 to 50 Degree. *J. Phys. Chem.* **1966**, *70*, 3820–3824. [CrossRef]

24. Miyagi, M.; Wan, Q.; Ahmad, M.F.; Gokulrangan, G.; Tomechko, S.E.; Bennett, B.; Dealwis, C. Histidine Hydrogen-Deuterium Exchange Mass Spectrometry for Probing the Microenvironment of Histidine Residues in Dihydrofolate Reductase. *PLoS ONE* **2011**, *6*, e17055. [CrossRef] [PubMed]

25. Tran, D.T.; Banerjee, S.; Alayash, A.I.; Crumbliss, A.L.; Fitzgerald, M.C. Slow Histidine H/D Exchange Protocol for Thermodynamic Analysis of Protein Folding and Stability Using Mass Spectrometry. *Anal. Chem.* **2012**, *84*, 1653–1660. [CrossRef] [PubMed]

26. Hayashi, N.; Kuyama, H.; Nakajima, C.; Kawahara, K.; Miyagi, M.; Nishimura, O.; Matsuo, H.; Nakazawa, T. Imidazole C-2 Hydrogen/Deuterium Exchange Reaction at Histidine for Probing Protein Structure and Function with Matrix-Assisted Laser Desorption Ionization Mass Spectrometry. *Biochemistry* **2014**, *53*, 1818–1826. [CrossRef] [PubMed]

27. Elferich, J.; Williamson, D.M.; David, L.L.; Shinde, U. Determination of Histidine pKa Values in the Propeptides of Furin and Proprotein Convertase 1/3 Using Histidine Hydrogen-Deuterium Exchange Mass Spectrometry. *Anal. Chem.* **2015**, *87*, 7909–7917. [CrossRef] [PubMed]

28. Mullangi, V.; Zhou, X.; Ball, D.W.; Anderson, D.J.; Miyagi, M. Quantitative Measurement of the Solvent Accessibility of Histidine Imidazole Groups in Proteins. *Biochemistry* **2012**, *51*, 7202–7208. [CrossRef] [PubMed]

29. Kimura, S.; Matsuo, H.; Narita, K. Hydrogen-Tritium Exchange Titration of the Histidine Residues in Ribonuclease Tl and Analysis of Their Microenvironments. *J. Biochem.* **1979**, *86*, 301–310. [CrossRef]

30. Minamino, N.; Matsuo, H.; Narita, K. Tritium Exchange Titration of Imidazole Derivatives—Factors Affecting on pKa and Reactivity of Imidazole Ring. In *Peptide Chemistry-1977*; Shiba, T., Ed.; Protein Research Foundation: Osaka, Japan, 1978; pp. 85–90.

31. Miyamoto, K.; Arata, Y.; Matsuo, H.; Narita, K. Hydrogen-Tritium Exchange and Nuclear Magnetic Resonance Titrations of the Histidine Residues in Ribonuclease St and Analysis of Their Microenvironment. *J. Biochem.* **1981**, *89*, 49–59. [CrossRef]

32. Bai, Y.; Milne, J.S.; Mayne, L.; Englander, S.W. Primary Structure Effects on Peptide Group Hydrogen Exchange. *Proteins* **1993**, *17*, 75–86. [CrossRef]

33. Dempsey, C.E. Hydrogen Exchange in Peptides and Proteins Using NMR-Spectroscopy. *Prog. Nucl. Magn. Reson. Spectrosc.* **2001**, *39*, 135–170. [CrossRef]

34. Miyagi, M.; Tanaka, K.; Watanabe, S.; Kondo, J.; Kishimoto, T. Identifying Protein-Drug Interactions in Cell Lysates Using Histidine Hydrogen Deuterium Exchange. *Anal. Chem.* **2021**, *93*, 14985–14995. [CrossRef] [PubMed]

35. Wimalasena, D.S.; Janowiak, B.E.; Lovell, S.; Miyagi, M.; Sun, J.; Zhou, H.; Hajduch, J.; Pooput, C.; Kirk, K.L.; Battaile, K.P.; et al. Evidence That Histidine Protonation of Receptor-Bound Anthrax Protective Antigen Is a Trigger for Pore Formation. *Biochemistry* **2010**, *49*, 6973–6983. [CrossRef] [PubMed]

36. Jørgensen, T.J.D.; Gårdsvoll, H.; Ploug, M.; Roepstorff, P. Intramolecular Migration of Amide Hydrogens in Protonated Peptides upon Collisional Activation. *J. Am. Chem. Soc.* **2005**, *127*, 2785–2793. [CrossRef] [PubMed]

37. Hamuro, Y.; Tomasso, J.C.; Coales, S.J. A Simple Test To Detect Hydrogen/Deuterium Scrambling during Gas-Phase Peptide Fragmentation. *Anal. Chem.* **2008**, *80*, 6785–6790. [CrossRef] [PubMed]

38. Abzalimov, R.R.; Kaplan, D.A.; Easterling, M.L.; Kaltashov, I.A. Protein Conformations Can Be Probed in Top-down HDX MS Experiments Utilizing Electron Transfer Dissociation of Protein Ions without Hydrogen Scrambling. *J. Am. Soc. Mass Spectrom.* **2009**, *20*, 1514–1517. [CrossRef]

39. Peters-Clarke, T.M.; Riley, N.M.; Westphall, M.S.; Coon, J.J. Practical Effects of Intramolecular Hydrogen Rearrangement in Electron Transfer Dissociation-Based Proteomics. *J. Am. Soc. Mass Spectrom.* **2022**, *33*, 100–110. [CrossRef]

40. Rand, K.D.; Adams, C.M.; Zubarev, R.A.; Jørgensen, T.J.D. Electron Capture Dissociation Proceeds with a Low Degree of Intramolecular Migration of Peptide Amide Hydrogens. *J. Am. Chem. Soc.* **2008**, *130*, 1341–1349. [CrossRef]

41. Brodie, N.I.; Huguet, R.; Zhang, T.; Viner, R.; Zabrouskov, V.; Pan, J.; Petrotchenko, E.V.; Borchers, C.H. Top-Down Hydrogen–Deuterium Exchange Analysis of Protein Structures Using Ultraviolet Photodissociation. *Anal. Chem.* **2018**, *90*, 3079–3082. [CrossRef]

42. Mistarz, U.H.; Bellina, B.; Jensen, P.F.; Brown, J.M.; Barran, P.E.; Rand, K.D. UV Photodissociation Mass Spectrometry Accurately Localize Sites of Backbone Deuteration in Peptides. *Anal. Chem.* **2018**, *90*, 1077–1080. [CrossRef]

43. James, E.I.; Murphree, T.A.; Vorauer, C.; Engen, J.R.; Guttman, M. Advances in Hydrogen/Deuterium Exchange Mass Spectrometry and the Pursuit of Challenging Biological Systems. *Chem. Rev.* **2022**, *122*, 7562–7623. [CrossRef]

44. Courouble, V.V.; Mann, M.D.; Griffin, P.R. Advances in Mass Spectrometry-Based Structural Proteomics: Development of HDX-MS and XL-MS Techniques from Recombinant Protein to Cellular Systems. *Isr. J. Chem.* **2023**, *63*, e202300084. [CrossRef]

45. Engen, J.R. Analysis of Protein Conformation and Dynamics by Hydrogen/Deuterium Exchange MS. *Anal. Chem.* **2009**, *81*, 7870–7875. [CrossRef] [PubMed]

46. Meng, Q.; Song, Y.-L.; Zhou, C.; He, H.; Zhang, N.; Zhou, H. A Hydrogen-Deuterium Exchange Mass Spectrometry-Based Protocol for Protein-Small Molecule Interaction Analysis. *Biophys. Rep.* **2023**, *9*, 99–111. [CrossRef] [PubMed]

47. Masson, G.R.; Burke, J.E.; Ahn, N.G.; Anand, G.S.; Borchers, C.; Brier, S.; Bou-Assaf, G.M.; Engen, J.R.; Englander, S.W.; Faber, J.; et al. Recommendations for Performing, Interpreting and Reporting Hydrogen Deuterium Exchange Mass Spectrometry (HDX-MS) Experiments. *Nat. Methods* **2019**, *16*, 595–602. [CrossRef] [PubMed]

48. Guillarme, D.; Heinisch, S.; Rocca, J.L. Effect of Temperature in Reversed Phase Liquid Chromatography. *J. Chromatogr. A* **2004**, *1052*, 39–51. [CrossRef] [PubMed]

49. Lundanes, E.; Greibrokk, T. Temperature Effects in Liquid Chromatography. *Adv. Chromatogr.* **2006**, *44*, 45–77.

50. Brüne, D.; Andrade-Navarro, M.A.; Mier, P. Proteome-Wide Comparison between the Amino Acid Composition of Domains and Linkers. *BMC Res. Notes* **2018**, *11*, 117. [CrossRef] [PubMed]

51. Miyahara, Y.; Shintani, K.; Hayashihara-Kakuhou, K.; Zukawa, T.; Morita, Y.; Nakazawa, T.; Yoshida, T.; Ohkubo, T.; Uchiyama, S. Effect of UVC Irradiation on the Oxidation of Histidine in Monoclonal Antibodies. *Sci. Rep.* **2020**, *10*, 6333. [CrossRef]

52. Lodowski, D.T.; Palczewski, K.; Miyagi, M. Conformational Changes in the G Protein-Coupled Receptor Rhodopsin Revealed by Histidine Hydrogen-Deuterium Exchange. *Biochemistry* **2010**, *49*, 9425–9427. [CrossRef]

53. de la Fuente, M.; Han, X.; Miyagi, M.; Nieman, M.T. Expression and Purification of Protease-Activated Receptor 4 (PAR4) and Analysis with Histidine Hydrogen–Deuterium Exchange. *Biochemistry* **2020**, *59*, 671–681. [CrossRef]

54. Cobb, N.J.; Apostol, M.I.; Chen, S.; Smirnovas, V.; Surewicz, W.K. Conformational Stability of Mammalian Prion Protein Amyloid Fibrils Is Dictated by a Packing Polymorphism within the Core Region. *J. Biol. Chem.* **2014**, *289*, 2643–2650. [CrossRef] [PubMed]

55. Safar, J.G.; Xiao, X.; Kabir, M.E.; Chen, S.; Kim, C.; Haldiman, T.; Cohen, Y.; Chen, W.; Cohen, M.L.; Surewicz, W.K. Structural Determinants of Phenotypic Diversity and Replication Rate of Human Prions. *PLoS Pathog.* **2015**, *11*, e1004832. [CrossRef] [PubMed]

56. Aguilar-Calvo, P.; Xiao, X.; Bett, C.; Eraña, H.; Soldau, K.; Castilla, J.; Nilsson, K.P.R.; Surewicz, W.K.; Sigurdson, C.J. Post-Translational Modifications in PrP Expand the Conformational Diversity of Prions In Vivo. *Sci. Rep.* **2017**, *7*, 43295. [CrossRef] [PubMed]

57. Li, Q.; Wang, F.; Xiao, X.; Kim, C.; Bohon, J.; Kiselar, J.; Safar, J.G.; Ma, J.; Surewicz, W.K. Structural Attributes of Mammalian Prion Infectivity: Insights from Studies with Synthetic Prions. *J. Biol. Chem.* **2018**, *293*, 18494–18503. [CrossRef]

58. Fitzgerald, M.C.; Jin, L.; Tran, D.T. Histidine Hydrogen Exchange for Analysis of Protein Folding, Structure, and Function. In *Hydrogen Exchange Mass Spectrometry of Proteins: Fundamentals, Methods, and Applications*; David, D.W., Ed.; John Wiley & Sons: Hoboken, NJ, USA, 2016; pp. 165–184.

59. Mullangi, V.; Mamillapalli, S.; Anderson, D.J.; Bann, J.G.; Miyagi, M. Long-Range Stabilization of Anthrax Protective Antigen upon Binding to CMG2. *Biochemistry* **2014**, *53*, 6084–6091. [CrossRef] [PubMed]

60. Cebo, M.; Kielmas, M.; Adamczyk, J.; Cebrat, M.; Szewczuk, Z.; Stefanowicz, P. Hydrogen-Deuterium Exchange in Imidazole as a Tool for Studying Histidine Phosphorylation. *Anal. Bioanal. Chem.* **2014**, *406*, 8013–8020. [CrossRef]

61. Dong, J.; Callahan, K.L.; Borotto, N.B.; Vachet, R.W. Identifying Zn-Bound Histidine Residues in Metalloproteins Using Hydrogen-Deuterium Exchange Mass Spectrometry. *Anal. Chem.* **2014**, *86*, 766–773. [CrossRef]

62. Dong, J.; Joseph, C.A.; Borotto, N.B.; Gill, V.L.; Maroney, M.J.; Vachet, R.W. Unique Effect of Cu(II) in the Metal-Induced Amyloid Formation of Beta-2-Microglobulin. *Biochemistry* **2014**, *53*, 1263–1274. [CrossRef]

63. Barlin, G.B.; Perrin, D.D. Dissociation Constants in the Elucidation of Structure. In *Elucidation of Organic Structures by Physical and Chemical Methods. Part I*; Bentley, K.W., Kirby, G.W., Eds.; Wiley: New York, NY, USA, 1972; pp. 611–677.

64. Nielsen, J.E.; Vriend, G. Optimizing the Hydrogen-Bond Network in Poisson-Boltzmann Equation-Based pKa Calculations. *Proteins Struct. Funct. Genet.* **2001**, *43*, 403–412. [CrossRef]

65. Findlay, D.; Herries, D.G.; Mathias, A.P.; Rabin, B.R.; Ross, C.A. The Active Site and Mechanism of Action of Bovine Pancreatic Ribonuclease. *Nature* **1961**, *190*, 781–784. [CrossRef]

66. Meadows, D.H.; Jardetzky, O. Nuclear Magnetic Resonance Studies of the Structure and Binding Sites of Enzymes. IV. Cytidine 3'-Monophosphate Binding to Ribonuclease. *Proc. Natl. Acad. Sci. USA* **1968**, *61*, 406–413. [CrossRef] [PubMed]

67. Wales, T.E.; Eggertson, M.J.; Engen, J.R. Considerations in the Analysis of Hydrogen Exchange Mass Spectrometry Data. *Methods Mol. Biol. Clifton NJ* **2013**, *1007*, 263–288. [CrossRef]

68. Narita, K.; Kangawa, K.; Kimura, S.; Miyamoto, N.; Minamino, N.; Matsuo, H. Microenvironment Around Histidine Residues in Ribonucleases Analyzed by Hydrogen-Tritium Exchange Titration. In *Frontier in Protein Chemistry*; Elsevier North Holland: New York, NY, USA, 1980; pp. 247–259.

69. Cuchillo, C.M.; Nogués, M.V.; Raines, R.T. Bovine Pancreatic Ribonuclease: Fifty Years of the First Enzymatic Reaction Mechanism. *Biochemistry* **2011**, *50*, 7835–7841. [CrossRef]

70. Raines, R.T. Ribonuclease A. *Chem. Rev.* **1998**, *98*, 1045–1066. [CrossRef] [PubMed]

71. Bradbury, J.H.; Chapman, B.E.; Crompton, M.W.; Norton, R.S.; Seng, J. Hydrogen-Deuterium Exchange of the C-2 Protons of Histidine and Histidine Peptides and Proteins. *J. Chem. Soc. Perkin Trans. 2* **1980**, 693–700. [CrossRef]

72. Rabenstein, D.L.; Sayer, T.L. Determination of Microscopic Acid Dissociation Constants by Nuclear Magnetic Resonance Spectrometry. *Anal. Chem.* **1976**, *48*, 1141–1146. [CrossRef]

73. Bystroff, C.; Kraut, J. Crystal Structure of Unliganded Escherichia Coli Dihydrofolate Reductase. Ligand-Induced Conformational Changes and Cooperativity in Binding. *Biochemistry* **1991**, *30*, 2227–2239. [CrossRef]

74. Sawaya, M.R.; Kraut, J. Loop and Subdomain Movements in the Mechanism of Escherichia Coli Dihydrofolate Reductase: Crystallographic Evidence. *Biochemistry* **1997**, *36*, 586–603. [CrossRef]

75. Yu, L.; Fesik, S.W. pH Titration of the Histidine Residues of Cyclophilin and FK506 Binding Protein in the Absence and Presence of Immunosuppressant Ligands. *Biochim. Biophys. Acta* **1994**, *1209*, 24–32. [CrossRef]

76. Markley, J.L. Correlation Proton Magnetic Resonance Studies at 250 MHz of Bovine Pancreatic Ribonuclease. II. The pH and Inhibitor-Induced Conformational Transitions Affecting Histidine-48 and One Tyrosine Residue of Ribonuclease A. *Biochemistry* **1975**, *14*, 3554–3561. [CrossRef]

77. Liu, T.; Ryan, M.; Dahlquist, F.W.; Griffith, O.H. Determination of pKa Values of the Histidine Side Chains of Phosphatidylinositol-Specific Phospholipase C from Bacillus Cereus by NMR Spectroscopy and Site-Directed Mutagenesis. *Protein Sci.* **1997**, *6*, 1937–1944. [CrossRef] [PubMed]